elsewhere,[10] these contacts imply donation of electron density to the silver atom. Finally, two $[(PPh_3)(C_6Cl_5)ClPt(\mu\text{-}Cl)Ag(PPh_3)]$ units are arranged in such a way that the bridging Cl1 atom of each unit is located at 3.023 (2) Å from the silver atom of the other unit, making a contact similar to that presented by the *o*-chlorine atom of the C_6Cl_5 groups. The distance between the silver atoms is 4.176 (2) Å, excluding any bonding interaction. Unfortunately, the low stability of these complexes in solution does not allow a molecular weight determination in order to establish if this weak interaction Cl1···Ag′ can be detected in solution. As for complex I and complex III, the formation of VI is the result of the interaction of two fragments, the platinum "$PtCl_2(C_6Cl_5)PPh_3$" and silver "$AgPPh_3$" moieties. However, some differences in the interactions of these moieties can be observed when the structures of the three complexes are compared. Table VI collects the main bond distances and angles. As may be seen, the interaction between the platinum and silver fragments is in the case of the anion in complex I mainly due to the Pt-Ag bond, with a very weak Pt-Cl-Ag bond, and two *o*-Cl···Ag contacts of the pentachlorophenyl groups. The interaction in the case of complex III is only due to the Pt-Cl-Ag bond, and neither Pt-Ag bonds nor *o*-Cl···Ag′ contacts are present. However, in complex VI the interaction between both fragments shows weaker Pt-Ag and stronger Pt-Cl-Ag bonds than in III. Moreover, in VI two contacts Ag···Cl, one to the *o*-Cl atom of the C_6Cl_5 group and the other to the bridging Cl1′, are detected.

Acknowledgment. We gratefully acknowledge the Direccion General de Investigación Científica y Tecnica for financial support (Project PB 85-0128) and for research grants (to I.A. and J.M.C.).

Supplementary Material Available: A full list of crystal data collection and refinement parameters, tables of bond distances and angles, anisotropic displacement parameters, and positional parameters, and a figure with the complete labeling scheme (6 pages); a table of observed and calculated structure factors (19 pages). Ordering information is given on any current masthead page.

(10) Usón, R.; Forniés, J.; Tomás, M. *J. Organomet. Chem.* **1988**, *358*, 525.

Contribution from the Departments of Chemistry, Louisiana State University, Baton Rouge, Louisiana 70803-1804, and Washington University, St. Louis, Missouri 63130

Preparation, Structure, and Redox Activity of Nickel(II), Palladium(II), and Copper(II) Cofacial Binuclear Bis(β-keto enamine) Complexes[§]

Julie R. Bradbury,[†] Jacqueline L. Hampton,[†] Daniel P. Martone,[‡] and Andrew W. Maverick*[,‡]

Received November 21, 1988

The synthesis of the new bis(β-keto enamine) ligand $BBIH_2$, or 5-*tert*-butyl-*m*-xylylenebis(acetylacetone imine) (3,3′-[5-(1,1-dimethylethyl)-1,3-phenylenebis(methylene)]bis(4-amino-3-penten-2-one)), and the properties of three of its cofacial binuclear metal complexes are described. $Ni_2(BBI)_2\cdot 2DMF$ ($Ni_2C_{50}H_{74}N_6O_6$; DMF = $(CH_3)_2NCHO$): monoclinic, space group $P2_1/c$ (No. 14); a = 13.091 (2), b = 11.206 (2), c = 18.015 (4) Å; β = 95.92 (1)°; Z = 2; R = 0.049 (R_w = 0.062) for 3583 reflections and 289 parameters. $Pd_2(BBI)_2\cdot 2DMF$ ($Pd_2C_{50}H_{74}N_6O_6$): monoclinic, space group $P2_1/c$ (No. 14); a = 13.251 (3), b = 11.196 (2), c = 17.962 (5) Å; β = 96.42 (2)°; Z = 2; R = 0.032 (R_w = 0.051) for 3850 reflections and 289 parameters. $Cu_2(BBI)_2\cdot 0.5CH_2Cl_2\cdot H_2O$ ($Cu_2C_{44.5}H_{63}ClN_4O_5$): monoclinic, space group $C2/m$ (No. 12); a = 26.802 (5), b = 9.887 (2), c = 9.021 (2) Å; β = 90.48 (1)°; Z = 2; R = 0.053 (R_w = 0.084) for 1634 reflections and 142 parameters. $Ni_2(BBI)_2\cdot 2DMF$ (Ni···Ni = 4.4305 (7) Å) and $Pd_2(BBI)_2\cdot 2DMF$ (Pd···Pd = 4.3471 (4) Å) are isostructural, with the *cis-anti*-$M_2(BBI)_2$ geometric isomer stabilized by weak hydrogen bonding to the DMF oxygen atoms. The high crystallographic symmetry of the metal complex in $Cu_2(BBI)_2$ (Cu···Cu = 4.321 (1) Å) has prevented identification of the specific $M_2(BBI)_2$ isomer present. $Ni_2(BBI)_2$ and $Cu_2(BBI)_2$ exhibit quasireversible two-electron-oxidation waves in cyclic voltammetry (CH_2Cl_2 solution), whereas the analogous mononuclear complexes M(acim)$_2$ (acimH = 2-amino-2-penten-4-one) show only irreversible one-electron oxidation. Initial electrochemical oxidation of $Pd_2(BBI)_2$, while involving only one electron, is ca. 0.4 V easier than that of Pd(acim)$_2$. Thus, the binuclear species exhibit new types of redox processes, and their relatively rigid structure appears to lead to unusual kinetic stability.

Introduction

We have recently begun investigating the chemistry of cofacial binuclear transition-metal complexes derived from bis(β-diketone) ligands. Our objective has been to combine the reactivity and geometric features of the cofacial diporphyrins[1] with the synthetic versatility of the β-diketone ligand. We first reported the preparation and properties of the *m*-xylylene-bridged copper(II) complex $Cu_2(XBA)_2$ (**1**; see Chart I).[2] We have also shown that the 2,7-dimethylnaphthalene derivative $Cu_2(NBA)_2$ is capable of intramolecular coordination of guest molecules (G; see structure **2**) such as 1,4-diazabicyclo[2.2.2]octane (Dabco)[3] and pyrazine.[4] We have also been interested in the effects of modified metal coordination environments on the redox properties of the complexes. In analogous mononuclear systems, for example, Schiff-base complexes such as M(acen) (**3**; see Chart I) show more facile redox processes[5] than the parent acetylacetone derivatives.[6,7]

[†] Washington University.

[‡] Louisiana State University.

[§] Ligand abbreviations: acacH = 2,4-pentanedione; acimH = acetylacetone imine (4-amino-3-penten-2-one); salimH = salicylaldimine; acenH_2 = bis(acetylacetone)ethylenediimine (4,4′-[1,2-ethanediyldinitrilo]bis(3-penten-2-one)); bzacenH_2 = bis(benzoylacetone)ethylenediimine (3,3′-[1,2-ethanediyldinitrilo]bis(1-phenyl-1-buten-2-one)); $XBAH_2$ = *m*-xylylenebis(acetylacetone) (3,3′-[1,3-phenylenebis(methylene)]bis(2,4-pentanedione)); $NBAH_2$ = 2,7-naphthalenediylbis(methylene)bis(acetylacetone) (3,3′-[2,7-naphthalenediylbis(methylene)]bis(2,4-pentanedione)); $BBAH_2$ = 5-*tert*-butyl-*m*-xylylenebis(acetylacetone) (3,3′-[5-(1,1-dimethylethyl)-1,3-phenylenebis(methylene)]bis(2,4-pentanedione)); $BBIH_2$ = 5-*tert*-butyl-*m*-xylylenebis(acetylacetone imine) (3,3′-[5-(1,1-dimethylethyl)-1,3-phenylenebis(methylene)]bis(4-amino-3-penten-2-one)).

(1) See, for example: Collman, J. P.; Kim, K.; Leidner, C. R. *Inorg. Chem.* **1987**, *26*, 1152-1157. Fillers, J. P.; Ravichandran, K. G.; Abdalmuhdi, I.; Tulinsky, A.; Chang, C. K. *J. Am. Chem. Soc.* **1986**, *108*, 417-424.

(2) Maverick, A. W.; Klavetter, F. E. *Inorg. Chem.* **1984**, *23*, 4129-4130.

(3) Maverick, A. W.; Buckingham, S. C.; Bradbury, J. R.; Yao, Q.; Stanley, G. G. *J. Am. Chem. Soc.* **1986**, *108*, 7430-7431.

(4) Maverick, A. W.; Ivie, M. L.; Fronczek, F. R. Manuscript in preparation.

(5) Cinquantini, A.; Seeber, R.; Cini, R.; Zanello, P. *J. Electroanal. Chem. Interfacial Electrochem.* **1982**, *134*, 65-73. Sulfur-containing ligands also lead to improved electrochemical properties: Chen, L. S.; Koehler, M. E.; Pestel, B. C.; Cummings, S. C. *J. Am. Chem. Soc.* **1978**, *100*, 7243-7248. Heath, G. A.; Leslie, J. H. *J. Chem. Soc., Dalton Trans.* **1983**, 1587-1592.

(6) Gritzner, G.; Murauer, H.; Gutmann, V. *J. Electroanal. Chem. Interfacial Electrochem.* **1979**, *101*, 177-183.

0020-1669/89/1328-2392$01.50/0

Chart I. Ligands and Metal Complexes[a]

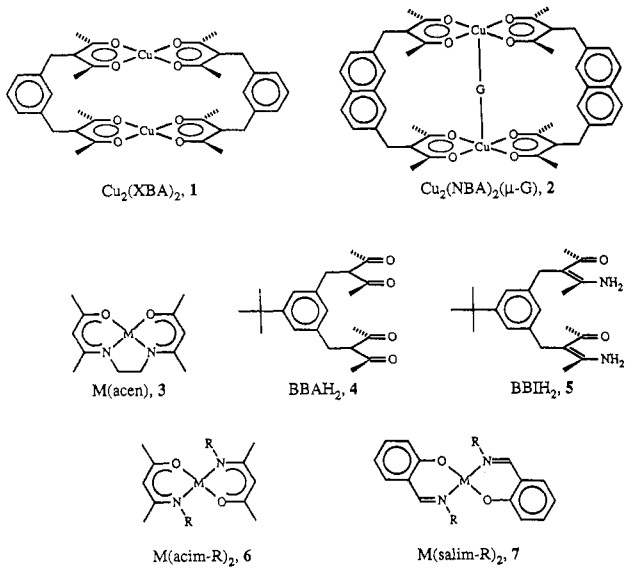

$Cu_2(XBA)_2$, 1 $Cu_2(NBA)_2(\mu\text{-}G)$, 2

M(acen), 3 $BBAH_2$, 4 $BBIH_2$, 5

M(acim-R)$_2$, 6 M(salim-R)$_2$, 7

[a] See text for abbreviations.

Chart II. Isomers of $M_2(BBI)_2$[a]

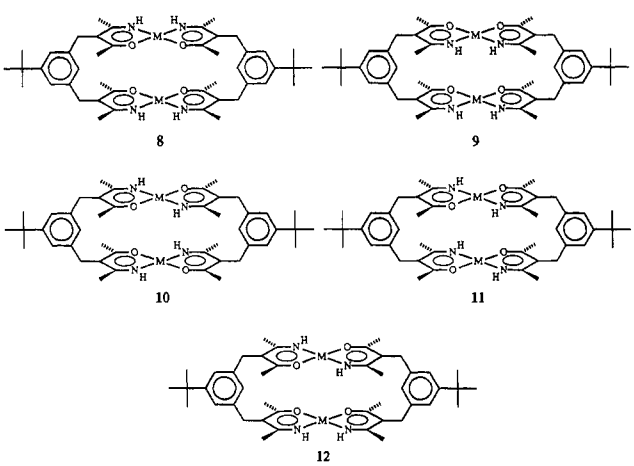

8 9 10 11 12

[a] Geometry: **8**, cis-anti; **9**, cis-syn; **10**, trans-anti; **11**, trans-syn; **12**, cis-trans. (**10** and **12** are chiral.)

As part of a general exploration of the nitrogen-containing derivatives of our binuclear systems, we have converted the new bis(β-diketone) $BBAH_2$ (**4**) to the bis(β-keto enamine) $BBIH_2$ (**5**) by treatment with NH_3, determined the structures of three cofacial binuclear bis(β-keto enamine) complexes $M_2(BBI)_2$ (see Chart II) by X-ray crystallography, and examined their redox properties by electrochemical methods. We find that the new complexes exhibit two types of oxidation–reduction behavior that are not observed in the corresponding mononuclear complexes.

Experimental Section

Materials and Procedures. Except during the synthesis of the bis(β-diketone) $BBAH_2$, no special precautions against reaction with O_2 or H_2O were required in the syntheses of the ligands and complexes. *tert*-Butyl alcohol (Mallinckrodt) was purified by distillation from potassium metal. For use in the inert-atmosphere drybox, dichloromethane was purified by distillation from CaH_2 under N_2. Literature procedures were used to prepare $(Bu_4N)(CF_3SO_3)$[8] and acimH and its Ni,[9] Cu,[10] and Pd[11] complexes **6** (R = H). Other chemicals and solvents were reagent or spectrophotometric grade and were used as received.

Electrochemical measurements were made by using a PAR Model 174A polarographic analyzer. The electrochemical cells employed Pt working (Bioanalytical Systems MF 2013 disk electrode; area 0.020 cm^2) and counter electrodes and a Ag/AgCl (3 M aqueous NaCl; Bioanalytical Systems MF2020) reference electrode (for experiments under ambient conditions in the laboratory) or a silver-wire pseudoreference electrode (for use in the drybox). The Fc/Fc^+ (Fc = ferrocene) couple was the reference redox couple; the half-wave potential for Fc/Fc^+ was 0.49 V vs Ag/AgCl under our conditions. The one-electron standard for cyclic voltammetry and stirred-solution normal-pulse voltammetry was $Ru(dbm)_3$ (dbmH = dibenzoylmethane).

^1H and ^{13}C NMR spectra were recorded by using Varian XL300 and Bruker AC100 and AC200 NMR spectrometers; chemical shift assignments for $BBAH_2$, $BBIH_2$, $Ni_2(BBI)_2$, and $Pd_2(BBI)_2$, along with those for the reference compounds $Ni(acim)_2$ and $Pd(acim)_2$, are tabulated in the supplementary material.

Preparation of Ligands. (a) 5-*tert*-Butyl-1,3-bis(bromomethyl)benzene was prepared by a modification of the method of Cram and co-workers.[12] A mixture of 5-*tert*-butyl-*m*-xylene (16.2 g; 0.10 mol) and *N*-bromosuccinimide (37.4 g; 0.21 mol) in 350 mL of CCl_4 was brought to reflux and benzoyl peroxide (0.3 g) added. After refluxing for 20 h, the mixture was cooled, filtered, washed with H_2O, dried over $MgSO_4$, and evaporated to dryness. The solid residue was recrystallized from cyclohexane to give white needles (yield 16–19 g, 50–60%).

(b) $BBAH_2$ (4). The general alkylation procedure of Martin and co-workers[13] was followed, except that we found substantial improvement in the quality of the product when the entire reaction was conducted under N_2. The following proportions were used: potassium, 3.62 g (0.0926 mol); *tert*-butyl alcohol, 200 mL; 2,4-pentanedione (acacH), 13.9 g (0.139 mol); 5-*tert*-butyl-1,3-bis(bromomethyl)benzene, 14.8 g (0.0463 mol); KI, 1.84 g. The reaction was complete after 72 h. Workup proceeded by distilling off nearly all of the *tert*-butyl alcohol, taking up the residue in CH_2Cl_2, washing with water, drying over $MgSO_4$, and evaporating to dryness. Excess acacH was removed under dynamic vacuum over a 16-h period. The product was an amber oil (yield 13–15 g, 80–90%). This material could be partially solidified by warming with pentane or methanol; ^1H NMR spectra showed that the resulting colorless crystalline solids were either a mixture of keto and enol forms (from pentane; mp 65 °C) or entirely in the keto form (from methanol; mp 80 °C).

(c) $BBIH_2$ (5). $BBAH_2$ was dissolved in the minimum volume of toluene and the solution dried over $MgSO_4$, warmed to 60 °C, and treated with NH_3(g) for 3–4 h. The container was then closed and left to stand for 16 h; at this point filtration gave a white powder (40–50% yield; a second crop of $BBIH_2$ could be isolated by drying the filtrate and treating it with NH_3 again), which was purified by crystallization from methanol–acetone. Anal. Calcd for $C_{22}H_{32}N_2O_2$: C, 74.12; H, 9.05; N, 7.86. Found: C, 74.16; H, 9.14; N, 7.61.

Metal Complexes of $BBIH_2$. (a) *cis-anti*-$Ni_2(BBI)_2$·2DMF. A solution of $Ni(NO_3)_2$·$6H_2O$ (0.081 g; 0.28 mmol) in DMF (20 mL) was added to a well-stirred solution of $BBIH_2$ (0.10 g; 0.28 mmol) and Et_3N (0.056 g; 0.56 mmol) in DMF (20 mL). The solution, which immediately turned red-brown, was left to stand; after 7–14 days, crystalline product suitable for X-ray analysis (yield 20–30%) was deposited. Anal. Cald for $Ni_2C_{50}H_{74}N_6O_6$: C, 61.75; H, 7.67; N, 8.64. Found: C, 61.73; H, 7.97; N, 9.08. When the reaction was carried out in methanol or with the reagents at higher concentrations, higher yields could be obtained. However, the product obtained under these conditions was not crystalline and was nearly insoluble in all common solvents. A powdery, soluble form of $Ni_2(BBI)_2$, whose NMR spectrum showed no evidence for DMF, was obtained by layering a CH_2Cl_2 solution of $Ni_2(BBI)_2$·2DMF with ethanol.

(b) *cis-anti*-$Pd_2(BBI)_2$·2DMF. A solution of $PdCl_2(CH_3CN)_2$ prepared by dissolving 0.200 g of $PdCl_2$ (1.13 mmol) in 50 mL of CH_3CN was added dropwise, with stirring, to a solution of $BBIH_2$ (0.400 g; 1.12 mmol) and Et_3N (0.228 g; 2.26 mmol) in 150 mL of CH_3CN. DMF (150 mL) was then added and the CH_3CN removed from the mixture under aspirator vacuum. The resulting bright yellow solution deposited solid $Pd_2(BBI)_2$·2DMF on treatment with four times its volume of methanol; if CH_3OH was layered on the DMF solution, crystals of the complex suitable for X-ray analysis were deposited. Anal. Calcd for $Pd_2C_{50}H_{74}N_6O_6$: C, 56.23; H, 6.98; N, 7.87. Found: C, 54.52; H, 6.91; N, 6.52. No impurities are evident in the ^1H or ^{13}C NMR spectra of this

(7) Related but more extensively substituted tetraaza macrocyclic complexes are also readily oxidized and reduced: Streeky, J. A.; Pillsbury, D. G.; Busch, D. H. *Inorg. Chem.* **1980**, *19*, 3148–3159.
(8) Maverick, A. W.; Najdzionek, J. S.; MacKenzie, D.; Nocera, D. G.; Gray, H. B. *J. Am. Chem. Soc.* **1983**, *105*, 1878–1882.
(9) Archer, R. D. *Inorg. Chem.* **1963**, *2*, 292–293.
(10) Lacey, M. J. *Aust. J. Chem.* **1970**, *23*, 841–842.
(11) Senda, Y.; Kasahara, A.; Suzuki, A.; Izumi, T. *Bull. Chem. Soc. Jpn.* **1976**, *49*, 3337–3338. Kasahara, A.; Izumi, T.; Sato, K.; Furukawa, K. *Bull. Yamagata Univ.* **1973**, *8*, 179–185.
(12) Moore, S. S.; Tarnowski, T. L.; Newcomb, M.; Cram, D. J. *J. Am. Chem. Soc.* **1977**, *99*, 6398–6405.
(13) Martin, D. F.; Fernelius, W. C.; Shamma, M. *J. Am. Chem. Soc.* **1959**, *81*, 130–133.

Table I. Crystallographic Data[a]

	$Ni_2(BBI)_2$·2DMF	$Pd_2(BBI)_2$·2DMF	$Cu_2(BBI)_2$·0.5CH_2Cl_2·H_2O
formula	$Ni_2C_{50}H_{74}N_6O_6$	$Pd_2C_{50}H_{74}N_6O_6$	$Cu_2C_{44.5}H_{63}ClN_4O_5$
a/Å	13.091 (2)	13.251 (3)	26.802 (5)
b/Å	11.206 (2)	11.196 (2)	9.887 (2)
c/Å	18.015 (4)	17.962 (5)	9.021 (2)
β/deg	95.92 (1)	96.42 (2)	90.48 (1)
V/Å^3	2628.8 (8)	2648 (1)	2390.5 (7)
Z	2	2	2
space group	$P2_1/c$ (No. 14)	$P2_1/c$ (No. 14)	$C2/m$ (No. 12)
ρ_x/g cm^{-3}	1.23	1.34	1.23
μ(Mo Kα)/cm^{-1}	7.67	7.18	9.90
$R(F_o)$	0.049	0.032	0.048
$R_w(F_o)$	0.062	0.051	0.082

[a] In Tables I–VI, estimated standard deviations in the least significant digits of the values are given in parentheses.

complex (see data in supplementary material); the poor analytical results for C and N may therefore reflect variations in amount of solvent of crystallization. Electrochemical experiments with the complex utilized crystalline material which was visibly indistinguishable from that used in the X-ray structure determination.

(c) $Cu_2(BBI)_2$. A solution of $BBIH_2$ (1.40 g; 3.9 mmol) and Et_3N (0.80 g; 7.8 mmol) in DMF (50 mL) was treated with a solution of 3.9 mmol of a copper(II) salt (either $Cu(O_3SCF_3)_2$[14] or commercially available $Cu(NO_3)_2$·3H_2O) in DMF (50 mL). The solution rapidly turned dark green and deposited a dark gray microcrystalline precipitate, which was collected, washed with DMF, and dried under dynamic vacuum. ^1H NMR spectra in $CDCl_3$ revealed that DMF was still present in the dry solid product even after extensive drying and washing with ethanol. Therefore, this product contains DMF of crystallization. Crystals of $Cu_2(BBI)_2$·0.5CH_2Cl_2·H_2O suitable for X-ray analysis were prepared from CH_2Cl_2 solutions of this material by layering with 2-propanol. Anal. Calcd for $Cu_2C_{44.5}H_{63}ClN_4O_5$: C, 59.62; H, 7.08; N, 6.25. Found: C, 60.86; H, 7.22; N, 6.26. (The observed analysis could be accommodated better by the formula $Cu_2(BBI)_2$·0.25CH_2Cl_2·H_2O, suggesting that the crystals slowly lose CH_2Cl_2. Calcd for $Cu_2C_{44.25}H_{62.5}ClN_4O_5$: C, 60.72; H, 7.20; N, 6.40.) The presence of CH_2Cl_2 in this material could be readily confirmed via ^1H NMR spectroscopy in $CDCl_3$. $Cu_2(BBI)_2$ is paramagnetic, so that its NMR spectrum is extensively broadened under these conditions; however, the CH_2Cl_2 resonance remains relatively sharp and is therefore easily detectable.

Data Collection and Structure Refinement. (a) General Remarks. Crystals were mounted in glass capillaries (to limit solvent loss, for $Pd_2(BBI)_2$·2DMF and $Cu_2(BBI)_2$·0.5CH_2Cl_2·H_2O) or on the end of a hollow glass fiber ($Ni_2(BBI)_2$·2DMF). Data for all three structures were collected at 23 ± 2 °C on a Nicolet P3 diffractometer fitted with a Mo Kα source and graphite monochromator (λ = 0.71069 Å), using the ω-scan method (variable scan rate, 2–29° min^{-1}). Final unit cell constants for each crystal were determined from the orientations of 15 centered high-angle reflections. Additional crystallographic data are summarized in Table I. Refined atomic coordinates for the three structures appear in Table II, and selected bond lengths and angles are in Tables III–VI.

The structures were solved by using the Enraf-Nonius SDP set of programs. The positions of the metal atoms were determined from Patterson maps, and the remaining non-hydrogen atoms were located from difference Fourier syntheses. Refinement was by full-matrix least squares; the function minimized was $\sum w(|F_o|-|F_c|)^2$. All non-hydrogen atoms, except for the solvent atoms in $Cu_2(BBI)_2$·0.5CH_2Cl_2·H_2O, were refined anisotropically. All hydrogen atoms were riding, with fixed isotropic displacement parameters. Initial positions of some of the hydrogen atoms, including those in the coordinated iminato groups and at least one in each methyl group, were determined from difference Fourier syntheses. These hydrogen atom positions suggested staggered H–C–C–C conformations both for the methyl groups in the β-keto iminato moieties (we observed similar angles in our previously reported bis(β-diketone) structures[2,3]) and for the *tert*-butyl groups. All other H atoms were placed in calculated positions by using the observed conformations as a guide for the methyl and *tert*-butyl groups. In the case of $Ni_2(BBI)_2$·2DMF, but not for the other two compounds, refining only the iminato H atom positional parameters by using low-angle data ($(\sin\theta)/\lambda$ < 0.3) led to some improvement. The environments about the iminato N atoms are essentially planar, with bond angles similar to those reported by Marongiu and Lingafelter[15] for Cu(salim)$_2$ (7, M = Cu, R = H).

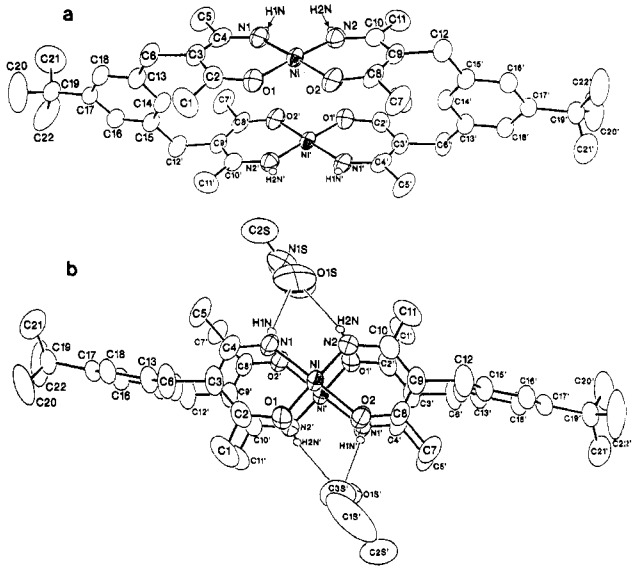

Figure 1. ORTEP[16] drawings for $Ni_2(BBI)_2$·2DMF, with thermal ellipsoids at the 50% probability level: (a) side view, including atom-labeling scheme (same scheme used for $Pd_2(BBI)_2$·2DMF); (b) top view, showing orientation of hydrogen-bonded DMF molecules. Primed and unprimed atoms are related by the crystallographic inversion center. Hydrogen bonds (Me_2NCHO---HN) are shown in single lines. Other hydrogen atoms are omitted for clarity.

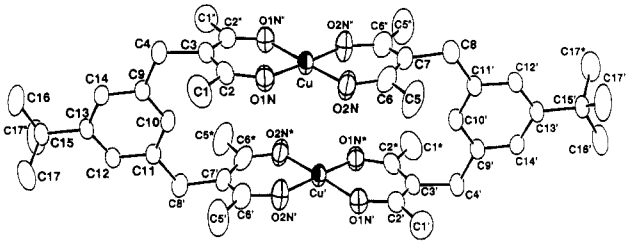

Figure 2. ORTEP[16] drawing for $Cu_2(BBI)_2$, with thermal ellipsoids at the 50% probability level. Atom-labeling scheme includes atoms X′, X″, and X*, related to X by crystallographic symmetry operations 2, m, and 2/m, respectively.

The crystal of $Pd_2(BBI)_2$·2DMF utilized for data collection was substantially larger (0.3 × 0.4 × 0.6 mm) than those of the Cu and Ni compounds (all dimensions 0.2–0.3 mm). Therefore, a correction for absorption, based on ψ scans for four reflections (calculated transmission coefficients 0.9318–0.9918), was applied to the data for $Pd_2(BBI)_2$·2DMF.

(b) $Ni_2(BBI)_2$·2DMF and $Pd_2(BBI)_2$·2DMF. The compounds are isostructural, with centrosymmetric $M_2(BBI)_2$ units. In initial refinement of these two structures, all four atoms coordinated to the metal atoms were assumed to be N. Isotropic displacement parameters for two of these atoms converged to substantially smaller values, as would be expected if N scattering factors were used to model O atoms. The resulting assignment of N and O atoms was confirmed both by the similarity of the N and O displacement parameters in the final structure and by the appearance of peaks in the difference Fourier maps corresponding to the iminato H atoms. Refinement converged at R = 0.049 (R_w = 0.062) and R = 0.032 (R_w = 0.051) for $Ni_2(BBI)_2$·2DMF and $Pd_2(BBI)_2$·2DMF, respectively. The structure and atom-numbering scheme for $Ni_2(BBI)_2$ are shown in the ORTEP[16] diagram in Figure 1, along with the orientation of the hydrogen-bonded DMF molecules. The same numbering scheme was used for $Pd_2(BBI)_2$·2DMF. No close intermolecular contacts were observed in either structure.

(14) Prepared from $CuCO_3$·$Cu(OH)_2$ and HO_3SCF_3: Howells, R. D.; McCown, J. D. *Chem. Rev.* **1977**, *77*, 69.

(15) Marongiu, G.; Lingafelter, E. C. *Acta Crystallogr., Sect. B* **1971**, *27B*, 1195–1201.

(16) Johnson, C. K. "ORTEP-II: A Fortran Thermal-Ellipsoid Plot Program for Crystal Structure Illustrations"; Report ORNL-5138; National Technical Information Service, U.S. Department of Commerce: Springfield, VA, 1976.

Table II. Refined Fractional Coordinates and Isotropic Equivalent Displacement Parameters[a]

atom	x	y	z	B_{eqv}, Å^2	atom	x	y	z	B_{eqv}, Å^2
				A. $Ni_2(BBI)_2$·2DMF					
Ni	0.09025 (5)	−0.01294 (6)	0.11069 (4)	3.59 (1)	C12	−0.1606 (4)	0.2159 (7)	0.2226 (3)	5.5 (1)
O1	0.1070 (3)	−0.1749 (4)	0.0983 (2)	4.59 (9)	C13	0.3557 (4)	−0.2644 (6)	−0.0535 (3)	4.4 (1)
O2	−0.0324 (3)	−0.0501 (4)	0.1465 (2)	4.81 (9)	C14	0.2662 (4)	−0.2357 (6)	−0.0977 (3)	4.5 (1)
N1	0.2121 (4)	0.0203 (5)	0.0749 (3)	4.7 (1)	C15	−0.2586 (4)	0.2489 (6)	0.1744 (3)	4.1 (1)
N2	0.0691 (4)	0.1468 (5)	0.1209 (3)	4.3 (1)	C16	−0.3430 (4)	0.2913 (5)	0.2073 (3)	3.9 (1)
C1	0.1698 (6)	−0.3658 (6)	0.0693 (4)	7.4 (2)	C17	0.4343 (4)	−0.3203 (5)	−0.1646 (3)	3.6 (1)
C2	0.1862 (5)	−0.2308 (6)	0.0765 (3)	4.4 (1)	C18	0.4382 (4)	−0.3062 (6)	−0.0875 (3)	4.1 (1)
C3	0.2758 (4)	−0.1772 (6)	0.0586 (3)	4.7 (1)	C19	−0.5287 (4)	0.3663 (6)	0.2003 (3)	4.4 (1)
C4	0.2833 (4)	−0.0537 (7)	0.0558 (3)	4.7 (1)	C20	0.5634 (7)	−0.4812 (8)	−0.1684 (5)	11.4 (2)
C5	0.3751 (5)	0.0070 (8)	0.0258 (4)	7.3 (2)	C21	0.6166 (6)	−0.278 (1)	−0.1856 (6)	11.7 (3)
C6	0.3605 (4)	−0.2525 (7)	0.0308 (3)	6.1 (2)	C22	−0.5100 (6)	0.377 (1)	0.2830 (4)	12.1 (3)
C7	−0.1908 (5)	−0.0363 (8)	0.1981 (4)	7.0 (2)	O1S	0.2087 (6)	0.2820 (8)	0.0163 (4)	11.9 (2)
C8	−0.0950 (4)	0.0226 (6)	0.1752 (3)	4.4 (1)	N1S	0.1900 (6)	0.3534 (6)	−0.1025 (4)	7.1 (2)
C9	−0.0826 (4)	0.1438 (6)	0.1840 (3)	4.3 (1)	C1S	0.1236 (9)	0.357 (1)	−0.1681 (6)	15.3 (4)
C10	−0.0033 (4)	0.2033 (6)	0.1521 (3)	4.3 (1)	C2S	0.2884 (8)	0.403 (1)	−0.0932 (6)	11.2 (3)
C11	−0.0004 (6)	0.3373 (7)	0.1497 (5)	7.1 (2)	C3S	0.1540 (8)	0.297 (1)	−0.0470 (5)	9.8 (3)
				B. $Pd_2(BBI)_2$·2DMF					
Pd	0.08732 (2)	−0.01405 (2)	0.10953 (1)	3.404 (5)	C12	−0.1615 (2)	0.2190 (4)	0.2250 (2)	4.85 (7)
O1	0.1074 (2)	−0.1887 (2)	0.0956 (1)	4.42 (4)	C13	0.3557 (2)	−0.2692 (3)	−0.0546 (2)	4.11 (6)
O2	−0.0437 (2)	−0.0514 (2)	0.1490 (1)	4.65 (5)	C14	0.2660 (2)	−0.2416 (3)	−0.0994 (2)	4.23 (6)
N1	0.2160 (2)	0.0202 (3)	0.0709 (2)	4.43 (6)	C15	−0.2587 (2)	0.2533 (3)	0.1768 (2)	3.85 (6)
N2	0.0643 (2)	0.1561 (2)	0.1213 (1)	4.11 (5)	C16	−0.3417 (2)	0.2960 (3)	0.2089 (2)	3.82 (6)
C1	0.1743 (3)	−0.3733 (3)	0.0664 (2)	6.29 (9)	C17	−0.4329 (2)	0.3234 (3)	0.1660 (2)	3.64 (6)
C2	0.1882 (2)	−0.2377 (3)	0.0741 (2)	4.28 (6)	C18	0.4378 (2)	−0.3093 (3)	−0.0883 (2)	4.04 (6)
C3	0.2744 (2)	−0.1825 (3)	0.0573 (2)	4.29 (6)	C19	−0.5263 (2)	0.3687 (3)	0.2011 (2)	4.54 (6)
C4	0.2838 (2)	−0.0586 (4)	0.0532 (2)	4.52 (7)	C20	−0.5605 (4)	0.4845 (4)	0.1672 (4)	10.5 (1)
C5	0.3758 (3)	−0.0013 (4)	0.0231 (3)	6.5 (1)	C21	−0.6152 (3)	0.2811 (6)	0.1816 (3)	10.1 (2)
C6	0.3596 (2)	−0.2578 (4)	0.0310 (2)	5.47 (8)	C22	−0.5074 (3)	0.3781 (6)	0.2846 (2)	10.2 (1)
C7	−0.1954 (3)	−0.0321 (4)	0.2013 (2)	6.50 (9)	O1S	0.2031 (3)	0.2186 (3)	0.5178 (2)	8.39 (9)
C8	−0.1007 (2)	0.0258 (3)	0.1780 (3)	4.37 (7)	N1S	0.1876 (3)	0.1538 (3)	0.3989 (2)	6.42 (8)
C9	−0.0852 (2)	0.1466 (3)	0.1863 (2)	4.01 (6)	C1S	0.1234 (5)	0.1477 (5)	0.3286 (3)	10.7 (2)
C10	−0.0078 (2)	0.2085 (3)	0.1527 (2)	4.07 (6)	C2S	0.2875 (4)	0.1030 (5)	0.4057 (3)	10.0 (2)
C11	−0.0064 (3)	0.3443 (3)	0.1527 (3)	6.31 (9)	C3S	0.1548 (3)	0.2087 (4)	0.4564 (3)	7.1 (1)
				C. $Cu_2(BBI)_2$·0.5CH_2Cl_2·H_2O					
Cu	0.04708 (2)	0	0.19559 (8)	3.91 (1)	C8	−0.1027 (2)	0	0.4878 (7)	5.0 (2)
O1N[b]	0.0936 (1)	−0.1361 (4)	0.1406 (3)	4.41 (7)	C9	0.2058 (2)	0	−0.1912 (6)	3.5 (1)
O2N[b]	0.0020 (1)	−0.1373 (4)	0.2579 (4)	5.37 (8)	C10	0.1586 (2)	0	−0.2602 (6)	3.9 (1)
C1	0.1643 (2)	−0.2536 (6)	0.0494 (6)	6.6 (1)	C11	−0.1536 (2)	0	0.4120 (6)	3.5 (1)
C2	0.1382 (2)	−0.1235 (5)	0.0849 (4)	4.08 (9)	C12	0.1964 (2)	0	−0.4992 (6)	3.3 (1)
C3	0.1612 (2)	0	0.0587 (6)	3.8 (1)	C13	0.2440 (2)	0	−0.4353 (6)	2.8 (1)
C4	0.2110 (2)	0	−0.0227 (6)	4.4 (1)	C14	0.2477 (2)	0	−0.2818 (6)	3.0 (1)
C5	−0.0621 (2)	−0.2560 (7)	0.3818 (8)	8.3 (2)	C15	0.2906 (2)	0	−0.5351 (6)	3.3 (1)
C6	−0.0380 (2)	−0.1228 (6)	0.3399 (5)	5.0 (1)	C16	0.3386 (3)	0	−0.4509 (8)	6.9 (2)
C7	−0.0572 (2)	0	0.3861 (6)	4.3 (1)	C17	0.2886 (2)	0.1235 (6)	−0.6376 (6)	6.5 (1)

[a] B_{eqv} is the isotropic equivalent displacement parameter $(4/3)[a^2\beta_{11} + b^2\beta_{22} + c^2\beta_{33} + ac(\cos\beta)\beta_{13}]$. [b] O and N atoms (occupancy 0.5 each), with positional and displacement parameters constrained to be equal.

Table III. Selected Bond Distances (Å) for $Ni_2(BBI)_2$·2DMF and $Pd_2(BBI)_2$·2DMF

	M			M	
	Ni	Pd		Ni	Pd
M–M	4.4305 (7)	4.3471 (4)	C3–C6	1.518 (4)	1.527 (4)
M–O1	1.845 (2)	1.994 (2)	C4–C5	1.527 (4)	1.529 (5)
M–O2	1.839 (2)	1.991 (2)	C6–C13	1.520 (4)	1.537 (4)
M–N1	1.819 (2)	1.950 (3)	C7–C8	1.511 (4)	1.514 (5)
M–N2	1.823 (2)	1.944 (3)	C8–C9	1.376 (4)	1.374 (5)
O1–C2	1.306 (3)	1.298 (4)	C9–C10	1.406 (4)	1.427 (5)
O2–C8	1.300 (4)	1.295 (4)	C9–C12	1.525 (4)	1.523 (4)
N1–C4	1.320 (4)	1.323 (5)	C10–C11	1.503 (5)	1.520 (5)
N2–C10	1.313 (3)	1.302 (4)	C12–C15	1.520 (4)	1.518 (4)
C1–C2	1.531 (5)	1.533 (5)	N1---O1S	3.116 (5)	3.074 (5)
C2–C3	1.385 (4)	1.362 (5)	N2---O1S	3.146 (4)	3.094 (4)
C3–C4	1.388 (5)	1.395 (5)			

Table IV. Selected Bond Angles (deg) for $Ni_2(BBI)_2$·2DMF and $Pd_2(BBI)_2$·2DMF

	M			M	
	Ni	Pd		Ni	Pd
O1–M–O2	86.5 (1)	88.4 (1)	C4–C3–C6	119.1 (3)	117.3 (3)
O1–M–N1	92.2 (1)	90.8 (1)	N1–C4–C3	124.3 (3)	125.7 (3)
O1–M–N2	177.9 (1)	178.4 (1)	N1–C4–C5	114.5 (3)	113.2 (4)
O2–M–N1	178.8 (1)	179.2 (1)	C3–C4–C5	121.1 (3)	121.0 (3)
O2–M–N2	92.3 (1)	90.8 (1)	C3–C6–C13	114.9 (2)	114.4 (2)
N1–M–N2	89.0 (1)	90.0 (1)	O2–C8–C7	114.2 (3)	111.4 (3)
M–O1–C2	128.1 (2)	125.3 (2)	O2–C8–C9	126.4 (3)	127.9 (3)
M–O2–C8	127.4 (2)	125.0 (2)	C7–C8–C9	119.5 (3)	120.7 (3)
M–N1–C4	129.2 (2)	126.7 (3)	C8–C9–C10	120.3 (3)	122.5 (3)
M–N2–C10	129.8 (2)	128.3 (2)	C8–C9–C12	119.9 (3)	118.4 (3)
O1–C2–C1	113.0 (3)	110.5 (3)	C10–C9–C12	119.5 (3)	118.7 (3)
O1–C2–C3	125.4 (3)	127.8 (3)	N2–C10–C9	122.8 (3)	124.2 (3)
C1–C2–C3	121.5 (3)	121.6 (3)	N2–C10–C11	116.7 (3)	116.2 (3)
C2–C3–C4	120.3 (3)	123.0 (3)	C9–C10–C11	120.5 (3)	119.6 (3)
C2–C3–C6	120.0 (3)	119.1 (3)	C9–C12–C15	115.7 (2)	116.0 (2)

(c) $Cu_2(BBI)_2$·0.5CH_2Cl_2·H_2O. The symmetry of the $Cu_2(BBI)_2$ unit in this crystal (see Figure 2) is $2/m$, with the mirror plane passing through Cu and carbon atoms 3, 4, and 7–16. As a result, the N and O atoms surrounding Cu cannot be distinguished. The two independent coordinated atoms, O1N and O2N, were therefore described as superposed O and N atoms, with occupancy 0.5 each, with positional and displacement parameters constrained to be equal. The high symmetry of the site suggested that the complex might have decomposed, possibly by hydrolysis to yield the more symmetrical bis(β-diketone) complex $Cu_2(BBA)_2$. However, the persistence of the keto iminato ligand was confirmed by microanalysis, by the appearance of peaks in the difference Fourier maps corresponding to the iminato H atoms (as in the Ni and Pd compounds), and by substantial electrochemical and electronic spectral differences between $Cu_2(BBI)_2$ and $Cu_2(BBA)_2$.

Refinement of only the $Cu_2(BBI)_2$ portion of the structure led to convergence at $R = 0.101$ ($R_w = 0.164$). At this point residual electron

Table V. Selected Bond Distances (Å) for $Cu_2(BBI)_2 \cdot 0.5CH_2Cl_2 \cdot H_2O$

Cu–Cu	4.321 (1)	C3–C4	1.529 (6)
Cu–O1N	1.904 (3)	C4–C9	1.526 (6)
Cu–O2N	1.906 (3)	C5–C6	1.517 (6)
O1N–C2	1.307 (4)	C6–C7	1.384 (5)
O2N–C6	1.315 (4)	C7–C8	1.532 (6)
C1–C2	1.500 (6)	C8–C11	1.519 (6)
C2–C3	1.389 (4)		

Table VI. Selected Bond Angles (deg) for $Cu_2(BBI)_2 \cdot 0.5CH_2Cl_2 \cdot H_2O$

O1N–Cu–O1N″	90.0 (2)	C2–C3–C2″	123.1 (4)
O1N–Cu–O2N	89.5 (1)	C2–C3–C4	118.2 (2)
O1N–Cu–O2N″	177.7 (1)	C3–C4–C9	113.9 (4)
O2N–Cu–O2N″	90.8 (2)	O2N–C6–C5	113.4 (4)
Cu–O1N–C2	129.5 (3)	O2N–C6–C7	124.9 (4)
Cu–O2N–C6	127.6 (3)	C5–C6–C7	121.7 (3)
O1N–C2–C1	115.5 (4)	C6–C7–C6″	122.5 (4)
O1N–C2–C3	123.9 (3)	C6–C7–C8	118.7 (2)
C1–C2–C3	120.6 (3)	C7–C8–C11	116.5 (4)

density (maximum difference Fourier peak height 2.43 e $Å^{-3}$) was apparent near the 2/*m* site at (0.5, 0, 0). This was modeled with two partially occupied disordered dichloromethane molecules (Cl1–C1Cl–Cl1 and Cl2–C1Cl–Cl2), with both Cl atoms in the $y = 0$ mirror plane and the common central atom C1Cl on a 2-fold axis ($x = 0.5$, $z = 0$) above and below the mirror plane. A partially occupied water molecule in the same mirror plane, represented by O1W, is also included in the model. The total occupancies correspond to one-half molecule of CH_2Cl_2 and one molecule of H_2O per $Cu_2(BBI)_2$ unit. According to this model, the region near (0.5, 0, 0) is occupied by either one dichloromethane molecule (in one of four possible orientations) or two water molecules; the distance O1W···O1W between the symmetry-related H_2O molecules is 4.15 Å.[17] Although the model accounted for much of the residual electron density, positional and displacement parameters could not be refined satisfactorily either for it or for several other plausible arrangements of partially occupied solvent molecules. Further refinement of the $Cu_2(BBI)_2$ positional and displacement parameters led to convergence with substantially improved discrepancy indices: $R = 0.048$; $R_w = 0.082$. Several intermolecular contacts (Cu···C7 = 3.784 Å; Cu···H8 = 2.82 Å; O2N···C6 = 3.758 Å) reflect the parallel alignment of adjacent $Cu_2(BBI)_2$ molecules in oblique "stacks" along the *c* axis. We observed similar but significantly closer intermolecular contacts in the structure of $Cu_2(NBA)_2 \cdot 2CHCl_3$;[3] the greater separation in $Cu_2(BBI)_2$ may be due to its saddle-shaped inward distortion (see Figure 2 and Discussion below).

Since the space group for $Cu_2(BBI)_2 \cdot 0.5CH_2Cl_2 \cdot H_2O$ was not uniquely determined by the diffraction data, we also attempted to refine models in the lower symmetry *C*2 and *Cm* space groups. Space group *C*2 was of particular interest because it would have eliminated the mirror plane relating the β-keto iminato O and NH moieties in the *C*2/*m* structure. This might therefore have made it possible to identify which $Cu_2(BBI)_2$ geometric isomer was present in the crystal. For each of the two attempts, starting coordinates for the non-hydrogen atoms were taken from the *C*2/*m* structure, with small shifts (maximum 0.05 Å) in randomly chosen directions to break the higher symmetry. In each case, refinement led to unreasonable and irregular bond distances in the $Cu_2(BBI)_2$ framework even when heavily damped. Large correlation coefficients were also observed in these attempted refinements between parameters related by the symmetry elements that had been removed (e.g. mirror-related parameters in the *C*2 trial). Therefore, we concluded that *C*2/*m* is the best space group for this structure.

Results

Synthesis of Ligands and Complexes. We originally prepared the *tert*-butyl-substituted bis(β-diketone) $BBAH_2$ (**4**) because the parent compound $XBAH_2$ was somewhat difficult to purify.[18] $BBAH_2$ is prepared by the nucleophilic substitution procedure originally developed by Martin and co-workers.[13] It is formed in two different modifications depending on the solvent used for crystallization. The solid obtained from methanol contains only the keto tautomer, whereas that from pentane contains both keto and enol forms. (We have observed this type of polymorphism in the unsubstituted bis(β-diketone) $XBAH_2$;[18] other bis(β-diketones) have also been obtained in more than one solid form.[13]) Solutions of either form of $BBAH_2$ in $CDCl_3$ gradually tautomerize, converting partly to the other form over a period of days. Both forms of $BBAH_2$ react with NH_3 to produce the bis(β-keto enamine) $BBIH_2$ (**5**).

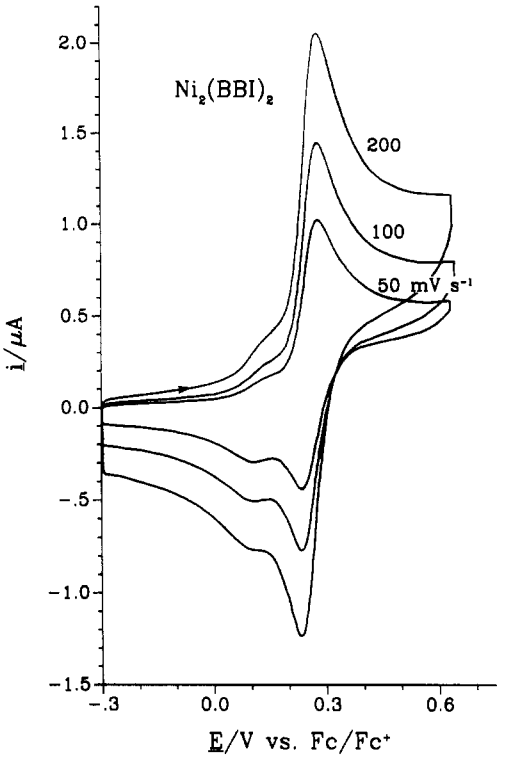

Figure 3. Cyclic voltammograms for $Ni_2(BBI)_2$ (1.6×10^{-4} M) in CH_2Cl_2, with 0.1 M $(Bu_4N)(O_3SCF_3)$ as supporting electrolyte (Pt working electrode; Ag-wire pseudoreference electrode).

The preparation of $Pd_2(BBI)_2$ and $Cu_2(BBI)_2$ is straightforward; there is no evidence for complications due to formation of polynuclear species. With nickel, the discrete binuclear complex $Ni_2(BBI)_2$ is the major product when the reactants are at low concentrations, but at higher concentrations and in solvents other than DMF much of the product appears in the form of powdery, insoluble materials that are probably polymeric. All three $M_2(BBI)_2$ complexes dissolve best in halogenated solvents, with solubilities in the order Cu > Pd > Ni. ^1H and ^{13}C NMR spectral data for the new ligands and for $Ni_2(BBI)_2$ and $Pd_2(BBI)_2$ are presented as supplementary material, along with data for acimH and its mononuclear Ni and Pd complexes.

General Description of the Structures. All three $M_2(BBI)_2$ complexes have a similar cofacial geometry. We were initially worried that the bis(β-keto enamine) ligand might lead to a mixture of $M_2(BBI)_2$ isomers. The five possible $M_2(BBI)_2$ isomers **8**–**12** are illustrated in Chart II, in which cis and trans describe the arrangement of O and NH around single metal atoms and syn and anti describe the relationship between the two metal environments. Because of their high symmetry, isomers **8**–**11** cannot be distinguished by simple techniques such as NMR chemical shift measurements. However, we have demonstrated by X-ray crystallography that the Ni and Pd complexes have the cis-anti structure **8**.

All three $M_2(BBI)_2$ structures contain nearly planar "$M(acim)_2$" moieties joined by 5-*tert*-butyl-*m*-xylylene bridges approximately at right angles (M = Ni, 85.4(2)°; M = Pd, 81.2(1)°; M = Cu, required to be 90° by symmetry). The metal–metal distances are 4.4305 (7) (M = Ni), 4.3471 (4) (M = Pd), and 4.321 (1) Å (M = Cu). In the Ni and Pd structures, *N*,*N*-dimethylformamide molecules lie near the centers of the $M_2(BBI)_2$ units (see drawing for $Ni_2(BBI)_2$ in Figure 1b, with the closest contact between the coordinated NH groups and the DMF O atoms (N···O =

(17) In this model, the $Cu_2(BBI)_2$ "O1N" and "O2N" atoms are at least 3.5 Å away from all of the solvent atoms; this argues against the type of H-bonding interaction observed in the Ni and Pd structures.

(18) Maverick, A. W.; Martone, D. P.; Bradbury, J. R.; Nelson, J. E. *Polyhedron*, in press.

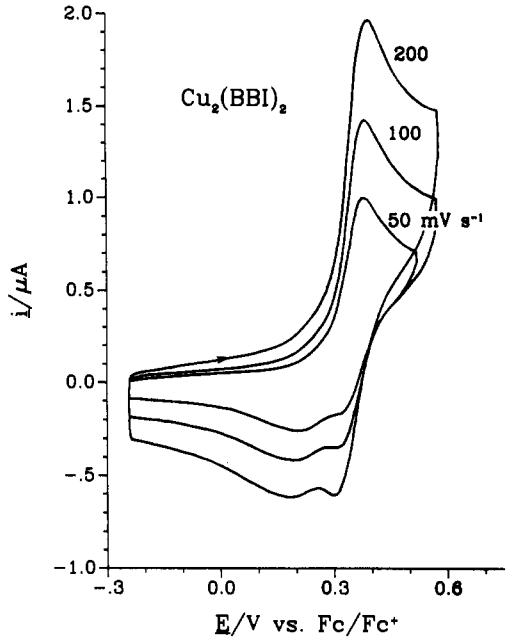

Figure 4. Cyclic voltammograms for $Cu_2(BBI)_2 \cdot 0.5CH_2Cl_2 \cdot H_2O$ (1.2×10^{-4} M) in CH_2Cl_2, with 0.1 M $(Bu_4N)(O_3SCF_3)$ as supporting electrolyte (Pt working electrode; Ag-wire pseudoreference electrode).

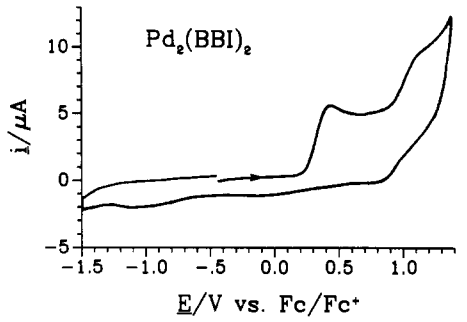

Figure 5. Cyclic voltammogram for $Pd_2(BBI)_2 \cdot 2DMF$ (7.6×10^{-4} M) in CH_2Cl_2, with 0.1 M $(Bu_4N)(O_3SCF_3)$ as supporting electrolyte (scan rate 200 mV s^{-1}; Pt working electrode; Ag/AgCl reference electrode).

3.07–3.15 Å). The DMF oxygen atoms are displaced out of the $M(acim)_2$ planes toward the centers of the complexes ($Ni_2(BBI)_2$, perpendicular distance 1.178 (8) Å, N–H---O angles 157 and 159°; $Pd_2(BBI)_2$, perpendicular distance 1.150 (3) Å, N–H---O angles 149 and 151°).

Electrochemistry. We have studied the electrochemical properties of the three new binuclear complexes by cyclic voltammetry and stirred-solution normal-pulse voltammetry. We have also compared their properties with those of the analogous mononuclear complexes $M(acim)_2$ (**6**, R = H). The results of these experiments are presented in Table VII; several cyclic voltammograms are reproduced in Figures 3–5. The data are concentrated on the first oxidation waves in all of the complexes, since these are the clearest and most readily accessible.

The electrochemical properties of $Cu_2(BBI)_2$ and $Ni_2(BBI)_2$ are similar. Both complexes, as originally prepared, contain DMF of crystallization. Solutions of these materials in CH_2Cl_2 exhibit two closely spaced quasireversible oxidation waves in cyclic voltammetry. However, the relative sizes of the two waves vary among different $M_2(BBI)_2$ samples; in some cases, the relative amplitudes change with time for a single sample. We suspected that the DMF in these materials, possibly including small amounts of DMF adsorbed on the surface of the solids, might be responsible for this variability in behavior. Therefore, we concentrated on materials that were free from DMF: crystalline $Cu_2(BBI)_2 \cdot 0.5CH_2Cl_2 \cdot H_2O$, as used in the X-ray structure determination, and a powdery, soluble form of $Ni_2(BBI)_2$. In both cases the absence of DMF was demonstrated by solution ^1H NMR spectra. These materials exhibited significantly improved and more reproducible electrochemical properties. For $Pd_2(BBI)_2$, however, the initial oxidation was found to be irreversible regardless of the method of preparation.

Table VII. Electrochemical Oxidation of Mononuclear and Binuclear β-Keto Enamine Complexes[a]

complex	scan rate/ V s^{-1}	$E_{1/2}$/ V[b]	i_{pc}/i_{pa}	ΔE_p/ mV[c]	$i_{pa}/(v^{1/2}AC_0^*)$[d]	$i_l/(AC_0^*)$[e]
$Ni_2(BBI)_2$	500	0.26	0.97	82	1350	1320
	200	0.26	0.84	74		
	100	0.26	0.81	63		
	50	0.26	0.73	56		
	20	0.25	0.60	47		
$Cu_2(BBI)_2$	500	0.36	0.95	167	1630	1550
	200	0.36	0.80	110		
	100	0.36	0.72	91		
	50	0.36	0.66	70		
	20	0.37	0.61	62		
$Pd_2(BBI)_2$	200	0.42[f]				560
$Ni(acim)_2$	200	0.52[f]				
$Cu(acim)_2$	200	0.61[f]				
$Pd(acim)_2$	200	0.66[f]				
$Ru(dbm)_3$[g]	100	−1.08	0.98	96	580	680

[a] Potentials vs Fc/Fc^+ in CH_2Cl_2. [b] $E_{1/2} = (E_{pa} + E_{pc})/2$. [c] $\Delta E_p = E_{pa} - E_{pc}$. [d] Average from data at several scan rates; i_{pa} in μA, A in cm^2; C_0^* in mol cm^{-3}. [e] From normal-pulse voltammetry, in A cm mol^{-1} (stirred solution; scan rate 20 mV s^{-1}, pulse rate 2 Hz); all other data from cyclic voltammetry. [f] Irreversible; value given is the anodic peak potential. [g] Data for $Ru(dbm)_3$ apply to its reversible one-electron reduction wave.

In addition to these initial oxidations, the complexes undergo reduction and further oxidation at more extreme potentials. Reductions are observed at −1.7, −1.9, and −1.5 V for $Cu_2(BBI)_2$, $Ni_2(BBI)_2$, and $Pd_2(BBI)_2$, respectively (all are E_{pc} values vs Fc/Fc^+); only the Cu complex shows a return wave ($E_{pa} = -1.0$ V). The second oxidations of the complexes occur at anodic peak potentials of 0.9 and 1.1 V for $Cu_2(BBI)_2$ and $Pd_2(BBI)_2$, respectively, with a small return wave at 0.8 V for $Cu_2(BBI)_2$; $Ni_2(BBI)_2$ shows only a gradually increasing anodic current beginning at ca. 0.9 V. Since these processes are superimposed on relatively large solvent background currents and are at best only partially reversible, they were not studied further.

Discussion

Formation of Complexes. Although the arrangement of O and NH groups in $Cu_2(BBI)_2$ cannot be determined from its crystal structure, the corresponding Ni and Pd complexes crystallize exclusively as the cis-anti isomer **8**. We attribute the preferential formation of **8** (M = Ni, Pd) in DMF solution to hydrogen bonding, as illustrated by the distances between the coordinated NH groups and the DMF oxygen atoms (N---O = 3.07–3.15 Å).[19] Of the possible $M_2(BBI)_2$ isomers **8**–**12**, the cis-anti isomer allows the greatest access by the relatively bulky DMF molecules; therefore, it probably exhibits the largest stabilization due to hydrogen bonding. We envision the preferential formation of *cis-anti*-$Ni_2(BBI)_2$, for example, as follows. The complex is initially produced as a mixture of isomers. However, it can isomerize readily in solution, by acid- or base-catalyzed processes. The lower solubility of the cis-anti isomer, in combination with DMF, gradually results in essentially complete conversion to **8**.

The capacity of the coordinated NH groups to function as hydrogen-bond donors is complementary to the O---$HCCl_3$ interaction we recently observed in the structure of the larger bis(β-diketone) complex $Cu_2(NBA)_2 \cdot 2CHCl_3$.[3] In the $Cu_2(NBA)_2 \cdot 2CHCl_3$ structure, the H-bonding interactions also occur substantially out of the β-diketone plane. The capacity of coordinated ketonato O atoms for the hydrogen bonding has previously been demonstrated in crystal structure analyses of Ni(acen)·$0.5H_2O$[20] and Cu(acen)·$0.5H_2O$.[21] Marongiu and Lin-

(19) Hamilton, W. C.; Ibers, J. A. *Hydrogen Bonding in Solids*; Benjamin: New York, 1968; p 16.
(20) Haider, S. Z.; Khan, M. S.; Hashem, A.; Riffel, H.; Hess, H. *Cryst. Struct. Commun.* **1982**, *11*, 1269–1275.

gafelter observed intermolecular hydrogen bonding involving coordinated iminato groups in the structure of *trans*-Cu(salim)$_2$ (**7**, M = Cu, R = H);[15] in contrast to our M$_2$(BBI)$_2$·2DMF structures, the NH---O linkages in Cu(salim)$_2$ are linear within experimental error.

Structural Flexibility. The metal–metal distances in the three M$_2$(BBI)$_2$ complexes (4.4305 (7) (M = Ni), 4.3471 (4) (M = Pd), and 4.321 (1) Å (M = Cu)) are significantly smaller than that in the closely related bis(β-diketone) complex Cu$_2$(XBA)$_2$ (4.908 (1) Å).[2] The shorter distances represent contractions of 0.6–0.7 Å relative to the *m*-xylylene carbon atoms in the bridging moieties (M = Ni, C6---C12′ = 5.040 Å; M = Pd, C6---C12′ = 5.052 Å; M = Cu, C4---C8′ = 5.090 Å; the corresponding distance in Cu$_2$(XBA)$_2$ is 5.081 Å). These contractions in metal–metal distances are the result of a slight saddle-shaped distortion in the "M(acim)$_2$" moieties in all three complexes; this distortion is noticeable in the Ni and Cu drawings of Figures 1 and 2. These structural results show that, although the *m*-xylylene bridging group provides a relatively rigid framework for the metal complexes, a substantial amount of flexibility remains in the metal–metal distance. Thus, the complexes should be able to accommodate small guest molecules of a variety of sizes.

Slight changes in the coordination environments of the three M$_2$(BBI)$_2$ complexes may be attributed to differences in the M–O and M–N bond lengths, which lie in the order Ni < Cu < Pd. As a result, Pd$_2$(BBI)$_2$ shows smaller O–M–N, M–N–C, and M–O–C angles, and larger C–C–C, C–C–N, and C–C–O angles, than those of Ni$_2$(BBI)$_2$. (The structure of Cu$_2$(BBI)$_2$ is difficult to compare in detail because of the disorder that is present.) Similar changes are observed in the structures of Ni(bzacen)[22] and Pd(bzacen).[23]

Cis–Trans Isomerism. The possibility of isomerism in M$_2$(BBI)$_2$ complexes has been mentioned above. In mononuclear systems, for example, the cis orientation of O and N is required in bridged species such as M(acen) (**3**), and planar complexes with two bidentate O, N ligands (e.g. **6** and **7**) must be trans except when R = H. Even in the least sterically hindered complexes **6** and **7** (i.e. R = H), the geometry has generally been assumed to be trans. Ni$_2$(BBI)$_2$ appears to be the first *cis*-N$_2$O$_2$ nickel(II) complex in which the N atoms are not constrained by a bridging group.

We have recently shown that Ni(acim)$_2$, the mononuclear species most closely related to the M$_2$(BBI)$_2$ complexes discussed here, is predominantly trans in solution,[24] with the cis and trans isomers in rapid equilibrium at room temperature. This isomerization probably occurs by twisting to produce a pseudotetrahedral intermediate of the type discussed by Holm and coworkers.[25] Mononuclear palladium(II) β-keto enamine complexes interconvert more slowly: Howie and Fay have isolated the cis and trans isomers of one such complex and studied their isomerization rates.[26] These interconversion rates are as expected, since the square-planar geometry is favored much more strongly over the pseudotetrahedral geometry in Pd(II) complexes.

Isomerization of Ni$_2$(BBI)$_2$ by the twisting mechanism discussed above is effectively blocked by the *m*-xylylene bridging groups. As a result, such an isomerization could probably only occur via partial or complete ligand dissociation. Although these are reasonable processes under the conditions of synthesis of the complexes (strongly coordinating solvent; relatively large quantities of acid and base present), they are unlikely with purified complexes in solvents such as CHCl$_3$ and CH$_2$Cl$_2$. Therefore, *cis-anti*-Ni$_2$(BBI)$_2$ probably does not isomerize when it is dissolved in chlorinated hydrocarbons. Steric repulsion probably also prevents isomerization of the other two M$_2$(BBI)$_2$ complexes after they are isolated and purified.

Electrochemistry. Our initial electrochemical studies of bis(β-diketone) complexes by cyclic voltammetry revealed only irreversible anodic and cathodic waves at extreme potentials. This was not surprising, since simple mononuclear β-diketone complexes such as Cu(acac)$_2$[27] and Pd(acac)$_2$[28] are also difficult to oxidize or reduce without decomposition. Replacement of the oxygen atoms in the coordination sphere of the mononuclear systems by atoms such as N and S, however, has been shown to improve their capacity for redox reactions.[5,7] Therefore, an important objective of the present work was to determine whether the redox properties of the binuclear systems could also be improved by introducing heteroatoms into the metal coordination sphere. We chose the bis(β-keto enamines) as the modified ligands because they represent a simple method for achieving N$_2$O$_2$ coordination at the metal atoms.

Ni$_2$(BBI)$_2$ and Cu$_2$(BBI)$_2$·0.5CH$_2$Cl$_2$·H$_2$O undergo quasireversible two-electron oxidation in CH$_2$Cl$_2$ solution, with half-wave potentials of 0.26 and 0.36 V vs Fc/Fc$^+$ respectively.[29] Typical cyclic voltammograms are shown in Figures 3 and 4, and electrochemical data are summarized in Table VII. The ratio of cathodic to anodic current, i_{pc}/i_{pa}, for the complexes approaches unity at higher scan rates, but in slower scans the return current is noticeably smaller. This suggests that the oxidized complexes are not completely stable on the electrochemical time scale, i.e. that electrooxidation is followed by conversion to other materials. In the case of Cu$_2$(BBI)$_2$, this other material appears to be electrochemically active (see below).

The assignment of these waves to two-electron processes could not be confirmed by bulk electrolysis, since the reactions are not chemically reversible. However, we have used normal-pulse voltammetry to determine *n*, by comparing the limiting currents for the anodic waves to that for one-electron reduction of Ru(dbm)$_3$ (whose electrochemical properties are well documented[30]) under the same conditions. Because the molecular weight of Ru(dbm)$_3$ (770.82) is close to those for Ni$_2$(BBI)$_2$ (826.38) and Cu$_2$(BBI)$_2$ (836.07), their diffusion coefficients D_0 are likely to be similar. Therefore, the limiting currents i_l in normal-pulse voltammetry[31] should be directly comparable. The results of this comparison (see Table VII) strongly suggest that both new complexes undergo two-electron oxidation.

The peak oxidation currents[32] observed in cyclic voltammograms for Ni$_2$(BBI)$_2$, Cu$_2$(BBI)$_2$, and Ru(dbm)$_3$ (see Table VII) also indicate that the binuclear complexes undergo two-electron oxidation.

Electrochemical oxidation of Ni$_2$(BBI)$_2$ and Cu$_2$(BBI)$_2$ can be viewed as consisting of two one-electron steps, with half-wave potentials $E_{1/2}(1)$ and $E_{1/2}(2)$. The shape of the observed wave in cyclic voltammetry is expected to depend on the difference $\Delta E_{1/2} = E_{1/2}(2) - E_{1/2}(1)$.[33] If the two oxidations are equivalent and independent of each other, oxidation of the two metal atoms is governed only by statistical factors (i.e. $\Delta E_{1/2}$ = 35.6 mV), and

(21) Clark, G. R.; Hall, D.; Waters, T. N. *J. Chem. Soc. A* **1968**, 223–226.
(22) Malatesta, V.; Mugnoli, A. *Can. J. Chem.* **1981**, *59*, 2766–2770.
(23) Malik, K. M. A.; Haider, S. Z.; Hashem, A.; Hursthouse, M. B. *Acta Crystallogr., Sect. C: Cryst. Struct. Commun.* **1985**, *C41*, 29–31.
(24) Maverick, A. W.; Fronczek, F. R.; Bradbury, J. R.; Martone, D. P. *J. Coord. Chem.*, in press.
(25) Holm, R. H.; O'Connor, M. J. *Prog. Inorg. Chem.* **1971**, *14*, 241–401 and references therein.
(26) Howie, J. K. Ph.D. Dissertation, Cornell University, 1977. In subsequent work the two isomers were characterized crystallographically: Fay, R. C. Personal communication.
(27) Gritzner, G.; Murauer, H.; Gutmann, V. *J. Electroanal. Chem. Interfacial Electrochem.* **1979**, *101*, 177–183.
(28) Hirota, M.; Fujiwara, S. *Bull. Chem. Soc. Jpn.* **1975**, *48*, 2825–2828.
(29) The ligand BBIH$_2$ undergoes irreversible oxidation at 0.68 V vs Fc/Fc$^+$ under comparable conditions.
(30) Endo, A. *Bull. Chem. Soc. Jpn.* **1983**, *56*, 2733–2738. Patterson, G. S.; Holm, R. H. *Inorg. Chem.* **1972**, *11*, 2285–2288. These authors studied the one-electron reduction of Ru(dbm)$_3$ in CH$_3$CN and DMF. The diffusion coefficient for Ru(dbm)$_3$ in CH$_3$CN has been determined (7.8×10^{-5} cm^2 s^{-1}): Takeuchi, Y.; Endo, A.; Shimizu, K.; Satô, G. P. *J. Electroanal. Chem. Interfacial Electrochem.* **1985**, *185*, 185–189.
(31) $i_l = nFAD_0C_0^*/\delta_0$ (where *n* electrons are transferred at an electrode of surface area *A*, C_0^* is the concentration of the reactant in the bulk solution, and δ_0 is the thickness of the steady-state Nernst diffusion layer). Adams, R. N. *Electrochemistry at Solid Electrodes*; Dekker: New York, 1969; p 70.
(32) The peak current is expected to be proportional to $n^{3/2}$: $i_p = (2.69 \times 10^5)n^{3/2}AD_0^{1/2}v^{1/2}C_0^*$. Bard, A. J.; Faulkner, L. R. *Electrochemical Methods: Fundamentals and Applications*; Wiley: New York, 1980; p 218.
(33) Myers, R. L.; Shain, I. *Anal. Chem.* **1969**, *41*, 980.

the observed peak separation will be the same as that ordinarily found for a reversible one-electron process, 59 mV. If the second electron transfer is assisted by the first (i.e. $\Delta E_{1/2} < 35.6$ mV), then the peak separation ΔE_p between anodic and cathodic waves will be smaller, approaching 30 mV when the second electron transfer is extremely favorable. The limiting values of ΔE_p at slow scan rates in our systems are ca. 40 and 60 mV for $Ni_2(BBI)_2$ and $Cu_2(BBI)_2$, respectively. This implies that there may be some cooperativity between the two successive oxidations of $Ni_2(BBI)_2$; on the other hand, the two oxidations of $Cu_2(BBI)_2$ are approximately independent of each other. The larger ΔE_p values we observe at higher scan rates may be due to uncompensated solution resistance;[34] especially for $Cu_2(BBI)_2$, they may also indicate that the electrode reactions are limited by the kinetics of electron transfer.

Additional smaller waves are observed in the voltammograms for both $Ni_2(BBI)_2$ (Figure 3) and $Cu_2(BBI)_2$ (Figure 4), at potentials slightly less positive than those for the principal oxidation. Because the major and minor waves overlap, we were unable to determine (by reversing the scan immediately after the minor oxidation wave) whether they are completely independent. With $Ni_2(BBI)_2$, the minor wave appears in both anodic and cathodic scans, and its amplitude relative to that of the major wave remains approximately constant over the range of scan rates we have studied. This suggests that the minor and major waves are independent of each other, and that the minor wave is the result of a small impurity in the $Ni_2(BBI)_2$ sample. (This impurity may be responsible for the fact that the anodic peak currents from cyclic voltammetry in Table VII for $Ni_2(BBI)_2$ are somewhat smaller than those for $Cu_2(BBI)_2$.) We observed similar but substantially larger secondary oxidation waves in voltammograms of $Ni_2(BBI)_2$·2DMF; thus, traces of DMF (or another donor molecule, such as H_2O) could be responsible for the minor wave in these experiments.

With $Cu_2(BBI)_2$, on the other hand, the additional wave appears only on the cathodic scan. Its amplitude relative to that of the major wave is largest at slow scan rates, suggesting that it is due to a material produced from electrogenerated $Cu_2(BBI)_2^{2+}$ on the time scale of a few seconds. Such a reaction would also be consistent with the smaller values of i_{pc}/i_{pa} observed at low scan rates. Coordination of a solvent or other donor (such as the triflate ion or traces of H_2O) to $Cu_2(BBI)_2^{2+}$ would explain these observations. In this system, however, the coordination would be necessary only in the oxidized form of the complex. Thus, $Cu_2(BBI)_2$, in its reduced form, may have a significant lower affinity for the donor molecule(s) than $Ni_2(BBI)_2$.

We attempted to determine whether these minor waves represent specific reactions with the supporting electrolyte by recording the voltammograms using $(Bu_4N)(BF_4)$ and $(Bu_4N)(PF_6)$ as supporting electrolytes. However, these voltammograms were inferior to those obtained with $(Bu_4N)(O_3SCF_3)$. For example, although $Ni_2(BBI)_2$ gave only a single oxidation wave with $(Bu_4N)(PF_6)$, ΔE_p values under these conditions were greater than 100 mV even at slow scan rates. Also, electrooxidation of $Cu_2(BBI)_2$ was only partially reversible with $(Bu_4N)(BF_4)$ and $(Bu_4N)(PF_6)$. We also investigated 1,2-dichloroethane as an alternative solvent (the complexes are insoluble in more convenient solvents such as CH_3CN and DMF). Again, although $Ni_2(BBI)_2$ gave a clean quasireversible oxidation wave in $C_2H_4Cl_2$, $Cu_2(BBI)_2$ still showed two overlapping return waves following oxidation, and the "minor" component was larger than that in CH_2Cl_2. Therefore, we concluded that $(Bu_4N)(O_3SCF_3)$ in CH_2Cl_2 gave the best combination of electrochemical properties for the new complexes.

The results described above for $Ni_2(BBI)_2$ and $Cu_2(BBI)_2$ may be compared with those for $Ni(acim)_2$ and $Cu(acim)_2$, also included in Table VII. The mononuclear complexes undergo only irreversible oxidation, probably by one electron, under the same conditions. Since the $Ni(acim)_2$ and $Cu(acim)_2$ reactions are irreversible, their anodic peak potentials are only approximately comparable with the half-wave potentials for the binuclear systems. However, it appears that the mononuclear and binuclear complexes provide similar environments for the formally divalent and trivalent metal ions. The improved electrochemical behavior of the binuclear Ni and Cu systems may be a result of their relatively rigid structure, which is a consequence of the *m*-xylylene bridging groups; this would represent an additional advantage for the cofacial binuclear systems.

With palladium as the central metal atom, both the mononuclear ($Pd(acim)_2$) and binuclear ($Pd_2(BBI)_2$) systems exhibit only irreversible electrochemical oxidation. The initial oxidation of $Pd_2(BBI)_2$·2DMF (see Figure 5) occurs at 0.42 V vs Fc/Fc^+ in CH_2Cl_2. Since the limiting current associated with this wave in normal-pulse voltammetry (560 A cm mol^{-1}) is very similar to that observed for $Ru(dbm)_3$ under the same conditions, we believe the wave represents one-electron oxidation. A qualitative comparison with $Pd(acim)_2$ (irreversible one-electron oxidation at 0.66 V vs Fc/Fc^+) suggests that initial oxidation of $Pd_2(BBI)_2$ is substantially easier than that for $Pd(acim)_2$. This may indicate some special stabilization for the formally Pd(II,III) mixed-valence complex $Pd_2(BBI)_2^+$, possibly by formation of a weak Pd–Pd bond.[35]

Summary. We have now modified our binucleating ligands to introduce nitrogen atoms into the metal coordination sphere, and we have characterized three cofacial binuclear complexes of one such bis(β-keto enamine) ligand. The binuclear complexes exhibit several improvements in their redox behavior as compared with simple mononuclear β-keto enamine complexes. Work currently in progress involves the extension of these redox processes to cofacial binuclear complexes of other metals, as well as the reactions of the complexes with small molecules such as O_2.

Acknowledgment is made to the donors of the Petroleum Research Fund, administered by the American Chemical Society, for support of this research. We thank John Waggenspack for experimental assistance. Funds for the Varian XL300 NMR instrument at Washington University were provided in part by NIH Biomedical Research Support Instrument Grant 1 S10 RR02004 and by a gift from the Monsanto Co.

Registry No. **4**, 120446-80-2; **5**, 120446-81-3; **6** (M = Ni, R = H), 25411-15-8; **6** (M = Cu, R = H), 69177-40-8; **6** (M = Pd, R = H), 51447-34-8; **8** (M = Ni), 120574-25-6; **8** (M = Pd), 120475-46-9; **8**·2DMF (M = Ni), 120475-45-8; **8**·2DMF (M = Pd), 120475-47-0; $PdCl_2(CH_3CN)_2$, 14592-56-4; $Cu_2(BBI)_2$, 120475-48-1; $Cu_2(BBI)_2$·$0.5CH_2Cl_2$·H_2O, 120475-49-2; $Ru(dbm)_3$, 15021-95-1; NH_3, 7664-41-7; 5-*tert*-butyl-1,3-bis(bromomethyl)benzene, 64726-28-9; 5-*tert*-butyl-*m*-xylene, 98-19-1; *N*-bromosuccinimide, 128-08-5.

Supplementary Material Available: For $Ni_2(BBI)_2$·2DMF, $Pd_2(BBI)_2$·2DMF, and $Cu_2(BBI)_2$·$0.5CH_2Cl_2$·H_2O, tables of ^1H and ^{13}C NMR spectral data, data collection and refinement parameters, anisotropic displacement parameters, calculated atomic coordinates and isotropic displacement parameters, peripheral bond distances and angles, and least-squares planes (13 pages); tables of observed and calculated structure factors (36 pages). Ordering information is given on any current masthead page.

(34) The value of ΔE_p given for $Ru(dbm)_3$ in Table VII (96 mV at 100 mV s^{-1}) is considerably larger than that expected (59 mV) for a reversible one-electron wave. This discrepancy is probably due to uncompensated resistance. Similar errors may be present in the data for the binuclear complexes, but to a lesser extent: the concentrations of $Cu_2(BBI)_2$ and $Ni_2(BBI)_2$ were substantially smaller (0.12 and 0.16 mM for $Cu_2(BBI)_2$ and $Ni_2(BBI)_2$, respectively, as compared with 1.01 mM for $Ru(dbm)_3$), so that the voltammetric peak currents were less than half as large for the binuclear complexes.

(35) These interactions are common in partially oxidized d^8 complexes. See, for example: Miller, J. S.; Epstein, A. J. *Prog. Inorg. Chem.* **1976**, *20*, 1–151. Clark, R. J. H.; Kurmoo, M.; Dawes, H.; Hursthouse, M. B. *Inorg. Chem.* **1986**, *25*, 409–412 and references therein.